PASSIVE TREATMENT OF LOW-PH, FERRIC IRON-DOMINATED ACID ROCK DRAINAGE IN A VERTICAL FLOW WETLAND II: METAL REMOVAL[1]

Robert C. Thomas and Christopher S. Romanek[2]

Abstract: A limestone-buffered organic substrate (LBOS) is used to passively remove iron (140 mg·L^{-1}) and aluminum (85 mg·L^{-1}) from low pH (<3), ferric iron-dominated acid rock drainage (ARD). Iron and aluminum removal is attributed to an increase in pH with precipitates of both elements segregated along a pH gradient. The increase in pH is rapid and occurs across a limestone dissolution front. Three distinct mineralogical zones demarcate the limestone dissolution front. The oxide zone overlies the dissolution front and contains organic material, iron oxyhydroxides, and quartz; all of the original limestone has been dissolved. Below the limestone dissolution front, the limestone is pristine and largely unreacted. Iron sulfides predominate. The zone of transition between iron oxyhydroxide and sulfide is also the zone of active limestone dissolution and the focus of aluminum precipitation.

Additional Key Words: limestone-buffered organic substrate, iron oxyhydroxide, aluminum hydroxysulfate, limestone dissolution, anaerobic wetland

_____

Introduction

Conventional wisdom holds that acid rock drainage (ARD) dominated by ferric iron cannot be treated directly by limestone; traditionally, some other mechanism must be invoked to convert the ferric iron to ferrous before contact with limestone. However, essential biological activity, including oxygen removal and reduction of ferric iron, is inhibited by the low pH typical of ferric iron-dominated ARD. Moreover, the reduction of ferric iron to ferrous ultimately leads to an increase in pH and a consequent decrease in the rate of limestone dissolution; as pH decreases, the rate of limestone dissolution increases proportionally (e.g., Plummer et al., 1979).

In the previous paper (Thomas and Romanek, 2002), we demonstrated that ferric iron-dominated ARD can be effectively treated using a vertical flow wetland (VFW) amended with a limestone-buffered organic substrate (LBOS). Limestone accounted for over 80% of the total alkalinity generated in the LBOS with dissolution occurring in a thin (2 – 5 cm) zone. Watzlaf (1997) also found that limestone dissolution occurs along a sharp reaction front in the compost layer of a reducing and alkalinity producing system (RAPS) – type VFW column study receiving low pH, ferric iron-dominated ARD. This dissolution front advances through the compost layer as the substrate's buffering capacity is consumed along the front (Thomas and Romanek, 2002; Watzlaf, 1997). Both studies observed apparent geochemical and mineralogical similarities above and below the reaction front that noteworthy.

Above the reaction front, the compost layer was orange due iron oxyhydroxides and the pH approached that of the influent ARD (pH <3). Below the reaction front, the pH was circumneutral, the same as the final effluent (Thomas and Romanek, 2002; Watzlaf, 1997). Aluminum precipitates were found concentrated at the reaction front where solubility of aluminum dropped from >100 $mg \cdot L^{-1}$ to <1 $mg \cdot L^{-1}$ due to the rapid change in pH (e.g., (Stumm and Morgan, 1981). Aluminum moved with the front, successively precipitating and dissolving with the changing pH conditions (Watzlaf, 1997). There was no indication that limestone dissolution was effected by ferric iron precipitates in the organic substrate, however influent iron (10 $mg \cdot L^{-1}$) and aluminum (18 $mg \cdot L^{-1}$) concentration were within limits for direct contact with limestone (e.g. <25 $mg \cdot L^{-1}$, Sterner et al., 1998).

The objective of this paper is to characterize metal attenuation processes in a VFW amended with limestone-buffered organic substrate (LBOS) and exposed to low pH (<3.0), ferric iron-

dominated ($Fe^{+3} \gg Fe^{+2}$) ARD. Thomas and Romanek (2002) provide details of a limestone dissolution front that develops in this LBOS over time. The dissolution front is demarcated by distinct mineralogical zonation, similar to Watzlaf's (1997) findings. In this paper, we describe the processes leading to the development of the mineralogical zonations. A model is presented for the evolution of these zones as the limestone dissolution front advances through the LBOS and predictions for long-term metal stability are made.

Materials and Methods

Substrate

The limestone buffered organic substrate (LBOS) was made by mixing 25% limestone screenings with 75% organic material by volume in small batches with a cement mixer. The cement mixer provided thorough mixing and homogenization of the limestone throughout the substrate. The screenings are high calcium limestone (91.5% by weight $CaCO_3$ as reported by the quarry) with a nominal grain size of 1.23 mm; greater than 80% of the screenings are between 0.59 and 4.76 mm. The organic material is a mixture of composted stable waste (96%), spent brewing grains (4%), and Kriket Krap® (composted cricket manure, <1%). The stable waste is composed of mainly wood shavings with minor amounts of straw and horse manure; it was collected from a refuse pile that was 3 to 5 years old.

Water Sampling and Analysis

Eight plastic tanks (92 cm diameter by 122 cm high) filled with 92 cm of LBOS overlying 15 cm of coarse (#57) limestone were used to simulate vertical flow wetlands. Details regarding sampling of the influent ARD and the VFW effluent are presented in the accompanying paper (Thomas and Romanek, 2002). Water samples were taken weekly from April 1999 to December 2000. Fine-scale pore water samples were collected using a vacuum-operated pore-water extractor (i.e., swamp suckers or swampers, Winger and Lasier, 1991) and acrylic pore-water diffusion samplers (i.e., peepers, Hesslein, 1976). Details on the construction and implementation of the swamper and peeper pore water samplers are presented in the accompanying paper (Thomas and Romanek, 2002).

The influent ARD was sampled for temperature, pH, acidity, sulfate, iron (Fe_T and Fe^{+2}), and dissolved metal content (Al, Fe, Mn, and Ca). The effluent was sampled for temperature, pH, alkalinity, dissolved metal content, sulfide, and sulfate. Swampers were sampled for temperature, pH, alkalinity, dissolved metal content, and sulfide. Due to the small sample volume, only temperature, pH, alkalinity, and dissolved metal content could be collected from using the peepers. Temperature and pH were measured in the field, dissolved sulfide (0.4 μm) was analyzed using a CHEMetrics™ sulfide test kit, acidity and alkalinity were determined in the lab by titration on unfiltered samples (APHA, 1998), sulfate was determined gravimetrically (APHA, 1998). Iron speciation was determined following a colorimetric FerroZine technique (To et al., 1999) that complexes ferrous iron. Samples for dissolved metals (0.4 μm) were analyzed by inductively coupled plasma mass spectrometry (ICP-MS). Only the major elements iron, aluminum, and calcium are reported in this study; trace metal chemistry is evaluated in (Thomas, 2002).

Substrate Sampling and Analysis

Substrate cores were extracted from a total of four different tanks for this study. Triplicate cores were taken from two tanks and replicates from two additional tanks. The ten cores were taken in the fall of 2000 near the end of the project. Substrate cores were handled in an anaerobic environment to prevent oxidation. Cores were divided into three subsamples (approximately 3-5 cm in length) based on three distinct color zonations (see results below). Subsamples were oriented in plastic cups, dried anaerobically, and vacuum-impregnated with epoxy. Polished substrate chips were prepared and examined with a JOEL electron microprobe using back-scatter electron (BSE) imaging. Precipitates were semi-quantitatively identified with an EDAX detector. Petrographic investigations were also conducted on dried samples of the initial substrate to provide baseline data.

Results

Influent Water Chemistry and Loading Rates

The influent is low pH (2.4), ferric iron-dominated ($Fe^{+3} \gg Fe^{+2}$) ARD. Primary contaminants are iron (average = 142 mg·L^{-1}), aluminum (average = 84 mg·L^{-1}), acidity (average = 1304 mg·L^{-1} as CaCO3 equivalents), and sulfate (average = 1521 mg·L^{-1}). The pH (average = 2.4) was consistent for the length of the project with little variation. Ferric iron averaged 96% of

the influent ARD total iron. Historic data indicate that the ARD is typically oxidized and highly acidic in nature (pH<3; e.g., Anderson, 1990; oxygen is near saturation, Millings, 1999; and iron is >95% ferric, Anderson et al., 1991).

Influent acidity ranged between 738 and 2320 mg·L^{-1} CaCO$_3$ equivalents. Given the consistency of the ARD pH, most of the variation in acidity can be assigned to changes in dissolved iron and aluminum concentration. The range in dissolved total iron and aluminum was 92 to 237 mg·L^{-1} and 39 to 274 mg·L^{-1}, respectively. Influent calcium concentrations were relatively low, averaging 52 mg·L^{-1} (23 to 114 mg·L^{-1} range).

Total acidity load received by any individual tank over the two years of the study averaged 18.6 Kg CaCO$_3$ equivalents; individual tanks received from 15.9 to 27.2 Kg CaCO$_3$ equivalents total acidity (see table 2, Thomas and Romanek, 2002). Total tank metal loading averaged 2.1 Kg for iron and 1.3 Kg for aluminum over the two years of the project. Total metal loads of individual tanks ranged from 1.6 to 3.3 Kg for iron and 1.0 to 1.9 Kg for aluminum. The area-adjusted loading rate for iron and aluminum was relatively low, averaging 7 and 4 g·d^{-1}·m^{-2}, respectively. With periodic high flows, however, a couple individual tanks experienced ephemeral iron loading rates over 100 g·d^{-1}·m^{-2} and aluminum loading of 50 g·d^{-1}·m^{-2} or more. Thomas (2002) showed that much of the variation in loading rates is due to flow and not changes in contaminant

Figure 1. Photograph of a split sediment core from the LBOS showing the three mineralogical zones overlying unreacted substrate. Scale to the right is in centimeters.

concentration. Loading on a volumetric basis was calculated according to (Eger, 1992), where the combined metal load equals the sum of the divalent metal load plus one and a half times the ferric iron and aluminum loads. Combined metal loading averaged 0.3 $moles \cdot d^{-1} \cdot m^{-3}$, with individual tank averages ranging from 0.2 to 0.4 $moles \cdot d^{-1} \cdot m^{-3}$.

Effluent Water Chemistry – Acidity Neutralization and Metal Removal

The average for all eight tanks presented in this section is calculated from the individual tank averages. Almost 90% of the iron and 100% of the aluminum and acidity were removed in the VFWs. The effluent is consistently circumneutral (average pH=6.4) and net alkaline (average=620 $mg \cdot L^{-1}$ $CaCO_3$ equivalents) with a fairly narrow range for both parameters. Effluent dissolved iron levels were an order of magnitude lower than the influent, averaging 15 $mg \cdot L^{-1}$ (2 to 33 $mg \cdot L^{-1}$ range in tank averages). For the majority of the effluent samples, the aluminum concentration was below the detection limit of the ICP-MS (approximately 0.03 $mg \cdot L^{-1}$ for aluminum), averaging only 0.05 $mg \cdot L^{-1}$ for the life of the project with a range in tank averages from 0.02 to 0.16 $mg \cdot L^{-1}$. Dissolved calcium increased more than an order of magnitude (average = 600 $mg \cdot L^{-1}$) as a result of limestone dissolution (see, Thomas and Romanek, 2002). Sulfate removal averaged approximately 320 $mg \cdot L^{-1}$ in the VFW or about 20% of the ARD influent sulfate. An average effluent sulfide value of 4.8 $mg \cdot L^{-1}$ was recorded with a seasonal average range of 0.3 to 22 $mg \cdot L^{-1}$. Effluent sulfide concentrations increased as the amount of sulfate removal increased, suggesting increases in removal were due to sulfate reduction.

Substrate Analysis – Core Description

Cores taken from the LBOS show a distinct color zonation (Figure 1). The upper 5-cm of true core material is orange due to the prevalence of iron oxyhydroxides. At approximately 5 cm, small irregular patches of buff-colored minerals are common and the color of the substrate changes fairly abruptly. The buff-colored minerals form a friable hardpan that cements between 2 – 5 cm of the LBOS immediately below the orange layer and is in sharp contact with a black zone that is notably lacking the buff-colored minerals. The black color, attributed to iron sulfides, extends a total of 5 – 10 cm and gradually fades into the brownish color of the original (unreacted) LBOS material below. Thus, the core can be divided into three basic reaction zones,

an upper orange layer of iron "oxides", a lower black layer of iron "sulfides", and an intermediary transitional zone demarcated by a hardpan of buff-colored minerals (Figure 1).

Pore Water – Swampers and Peepers

Based on preliminary observations of the core substrate, swamper samples were collected at three depths (1.5, 7.5, and 15 cm) in an effort to approximate the chemistry of the three color-zones. Peepers were inserted in the substrate, so that two wells sampled the water column and five wells sampled the substrate at 5-cm intervals starting just below the substrate-water interface. Without being able to determine the exact thickness and depth of each zone prior to sampling, there is no way of knowing the correlation between the swamper and peeper data and the three mineralogical zones. The swamper and peeper pore water samples are at best "operationally defined".

Both swamper and peeper data indicate pH increases sharply to effluent values (6.8) above 23 cm (Figure 2). Swamper samples show that removal of both iron and aluminum (Figures 2) is concurrent with the increase in pH, occurring above 7.5 cm in the LBOS. Peeper data also shows most of the dissolved iron and aluminum is removed in the upper 23 cm of the LBOS, however effluent levels of iron and aluminum are not reached until 22.5 cm and 12.5 cm deep, respectively (Figures 2 – 3). Both iron and aluminum increase with depth, peaking at concentrations more than double that of the overlying ARD water column, before showing rapid removal to effluent concentrations (i.e., Fe ~ 20 mg·L^{-1}; Al < 0.2 mg·L^{-1}). Aluminum values peaked at 7.5 cm and removal was accomplished within 5 cm, whereas iron peaked at 12.5 cm and complete removal occurred within 10 cm. Concomitant with the increase in dissolved iron (Figure 4), iron speciation shifts from ferric dominated in the overlying ARD water column to ferrous dominated by 2.5 cm; the water is greater than 90% ferrous by 7.5 cm. In fact, both peeper and swamper data indicate that iron is greater than 75% ferrous by 2.5 cm (Figure 2).

Although highly variable at any given depth, in general, the amount of dissolved calcium increases rapidly within the upper 12.5 cm of the LBOS (Figure 3). Calcium measured in the swamper samples just below the substrate-water interface is approximately double the influent concentration. Calcium concentrations nearly double again, approaching effluent values (~ 650 mg·L^{-1}), by 7.5 cm deep (Figure 3). Pore water for calcium analysis was collected with the peepers several months after the swamper samples were collected. Peeper calcium levels show a
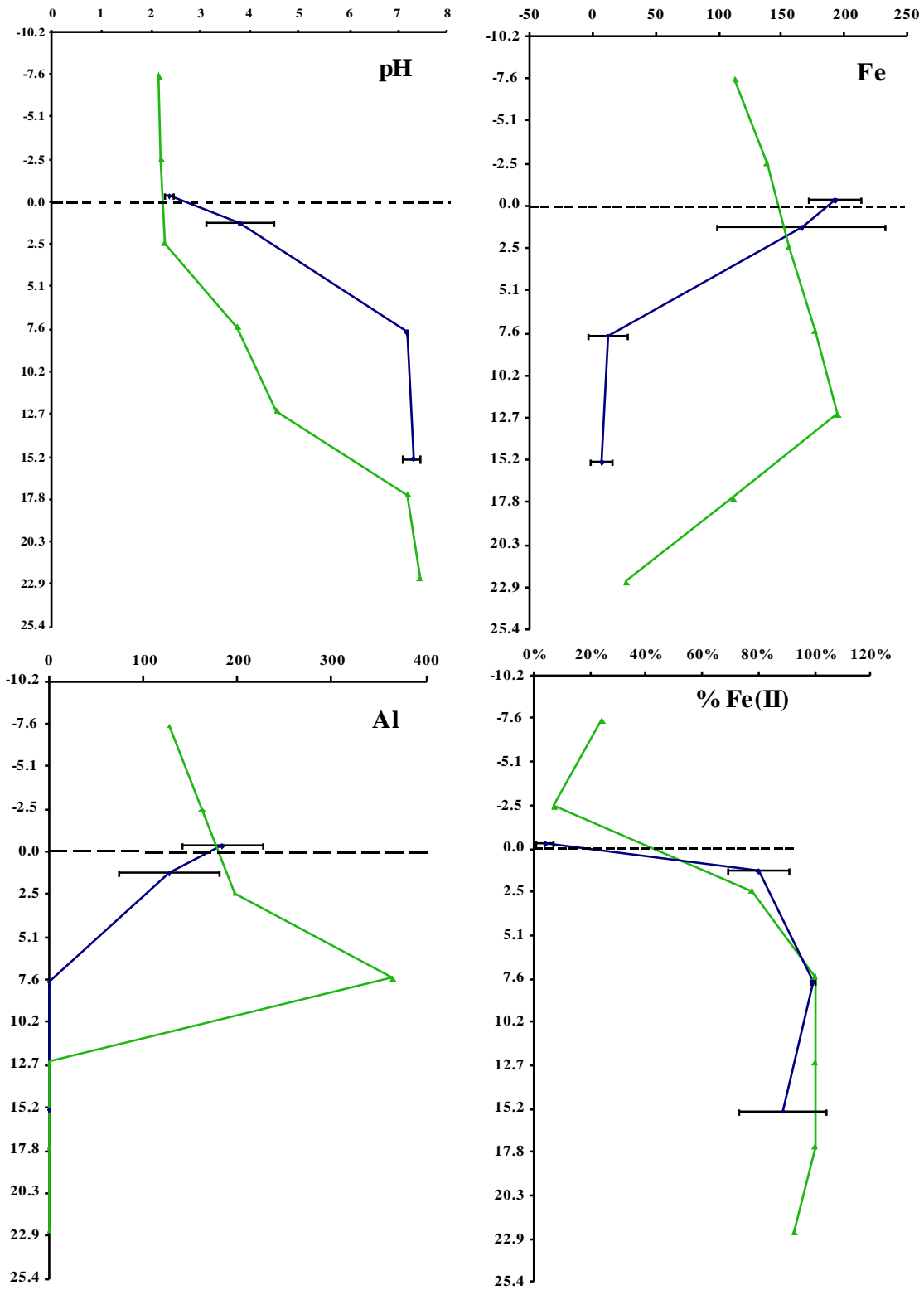
Figure 2. Pore water pH, iron, aluminum, and percent ferrous iron in the upper LBOS sampled with swampers and peepers (negative values represent samples from the ARD water-column overlying the LBOS).
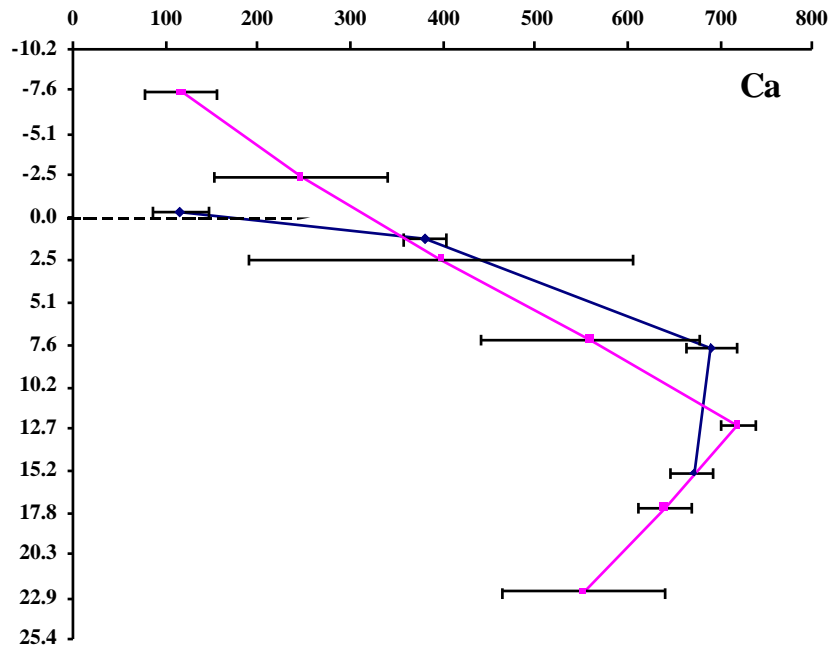
Figure 3. Pore water calcium in the upper LBOS sampled with swampers and peepers (negative values represent samples from the ARD water-column overlying the LBOS).

similar trend of rapid increase. However, peeper calcium values peak 12.5 cm deep in the LBOS at values over 200 mg·L^{-1} greater than measured effluent concentrations (~ 500 mg·L^{-1}). The amount of calcium rapidly drops to effluent concentrations over the next 10 cm (Figure 3).

Substrate Analysis – Electron Microprobe

Original substrate. Analysis of the original substrate was conducted to catalog the initial textures of the organic material and limestone and check for any preexisting metal precipitates. According to the size analysis of the limestone screenings provided by the quarry, less than one percent is smaller than 150 micrometers.   However, limestone fragments less than 10 micrometers are ubiquitous (Figure 4). Fragments are found rimming most large (> 100μm) particles (i.e., quartz, organic matter, and limestone; Figure 4a) and within cavities of the larger limestone fragments (Figure 4b – c). Occasional pieces of pyrite are observed, almost solely associated with limestone. Most are anhedral and larger than 50 μm, although rare pyrite framboids (10 – 20 μm diameter) are noted in some of the limestone cavities (Figure 4b); framboids were never identified with the organic matter.

760

<u>Oxide zone</u>. Visually, the oxide layer is fairly nondescript; organic fragments and orange iron oxyhydroxide precipitates are the only discernible components in a hand sample. Back-scatter imaging shows that the oxide zone is comprised of a series of chemically and/or texturally unique layers (Figure 5). The upper most portions of the oxide zone contain only three components: organic (largely wood) fragments, iron oxyhydroxides, and quartz (Figure 5a). There is no limestone present (e.g., Thomas and Romanek, 2002). The iron oxyhydroxides display textures indicative of rapid precipitation (dendritic growth, Figure 5b) and gel growth (blue arrows, Figure 5a). Gel textures occur in open voids between grains, while dendritic growth habits nucleate from existing surfaces (wood fragments, quartz grains). In addition to the dendritic coatings, iron is found rimming almost all organic fragments (Figure 5a), often permineralizing the outer edges of the fragment (Figure 5c). Dendritic forms are also found nucleating from the convex side of arcs that partially enclosed empty space, suggesting iron

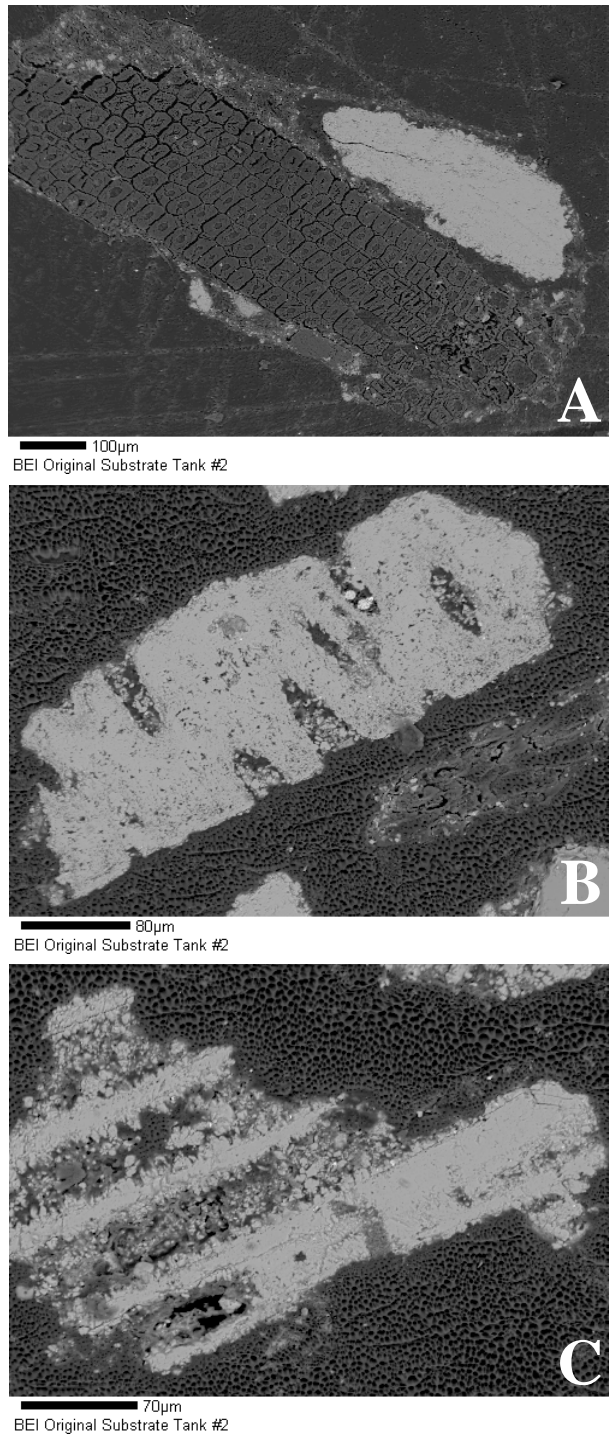

Figure 4. Photomicrographs of the original substrate. (A) Organic fragment adjacent to coarse grained limestone, note the fine-grained (<10μm) limestone surrounding both grains. (B) Limestone fossil fragment with fine-grained limestone in cavities. (C) Fine-grained limestone attached to a shell fragment.
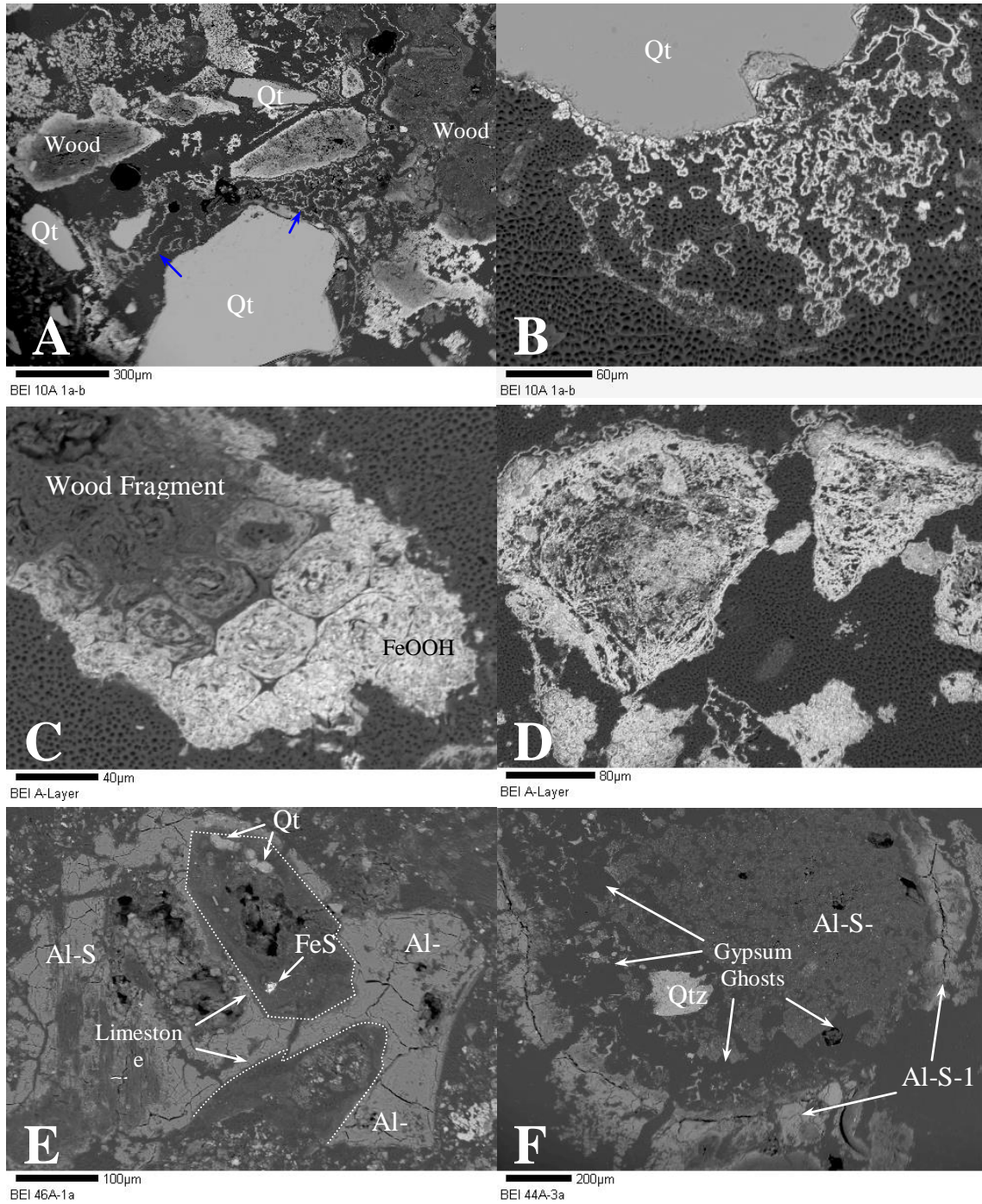
Figure 5. Photomicrographs of the oxide zone. (A) Iron textures of the upper oxide zone. Note the organic fragments permineralized along the outer edge and the dendritic oxyhydroxide textures indicative of rapid precipitation (B) Dendritic iron oxyhydroxides coating a quartz grain. (C) Permineralized organic fragment. (D) Skeletal replacement of limestone by iron oxyhydroxide with mammarian overgrowths of oxyhydroxide. (E) Patch of aluminum hydroxysulfate in the lower oxide zone outlining several limestone ghosts. Note no remnant limestone is present. (F) Another limestone ghost outlined and partially filled by aluminum hydroxysulfate. The former presence of blocky gypsum grains is preserved by the later aluminum hydroxysulfate.

oxyhydroxides coated grains that were subsequently dissolved away. Irregular and kidney-form patches of dendritic iron oxyhydroxide typically occur within the boundary of former grains (Figure 5a). Apparent skeletal replacement also occurs; former grains are outlined by mammarian-textured iron coatings and completely replaced by sinuous skeletal-iron oxyhydroxide (Figure 5d).

While absent from the very upper portions of the oxide layer, aluminum hydroxysulfates occur with increasingly greater frequency towards the bottom of the oxide layer. The aluminum hydroxysulfates initially occur intergrown with bands of dendritic iron oxyhydroxide, but with depth occur more frequently as very small (<500 μm), isolated patches and arced bands. The patches often contain subrounded voids (Figure 5e) and the bands are usually arranged in a circular manner around an open space with aluminum hydroxysulfates thinly dispersed in the interior (Figure 5f). Based on evidence presented in the transitional zone (see below), the cavities outlined by the aluminum hydroxysulfates are limestone ghosts (i.e., the visible outline of a former crystal shape, Figure 5e). Limestone, however, is still absent from the lower portions of the oxide zone. Rare pyrite occurs in the lower portions of the oxide zone and is commonly associated with limestone ghosts (Figure 5e). It is not known whether the pyrite is authigenic or residual from the former limestone grain.

Transitional zone. The boundary between the oxide layer and the transitional zone is characterized by a rapid shift from iron- to aluminum-dominated coatings and textures. Iron oxyhydroxides are still present in the upper portions of the transitional zone, but as isolated patches and intergrowths within bands of aluminum hydroxysulfate. Abundant limestone ghosts outlined by aluminum hydroxysulfate are typical in the upper portions of the transitional zone (Figure 6a), although they are largely devoid of limestone. Crystalline gypsum is occasionally observed within the boundary of the limestone ghosts (Figure 6b). Partially dissolved, the gypsum occurs as subrounded grains sparsely scattered within the bounds of former limestone fragments. The original euhedral, blocky shape of the gypsum is commonly preserved by aluminum hydroxysulfates (Figure 6c). These aluminum precipitates outline gypsum ghosts within remnant limestone grains in the lower portions of the oxide zone (e.g., Figure 5f).
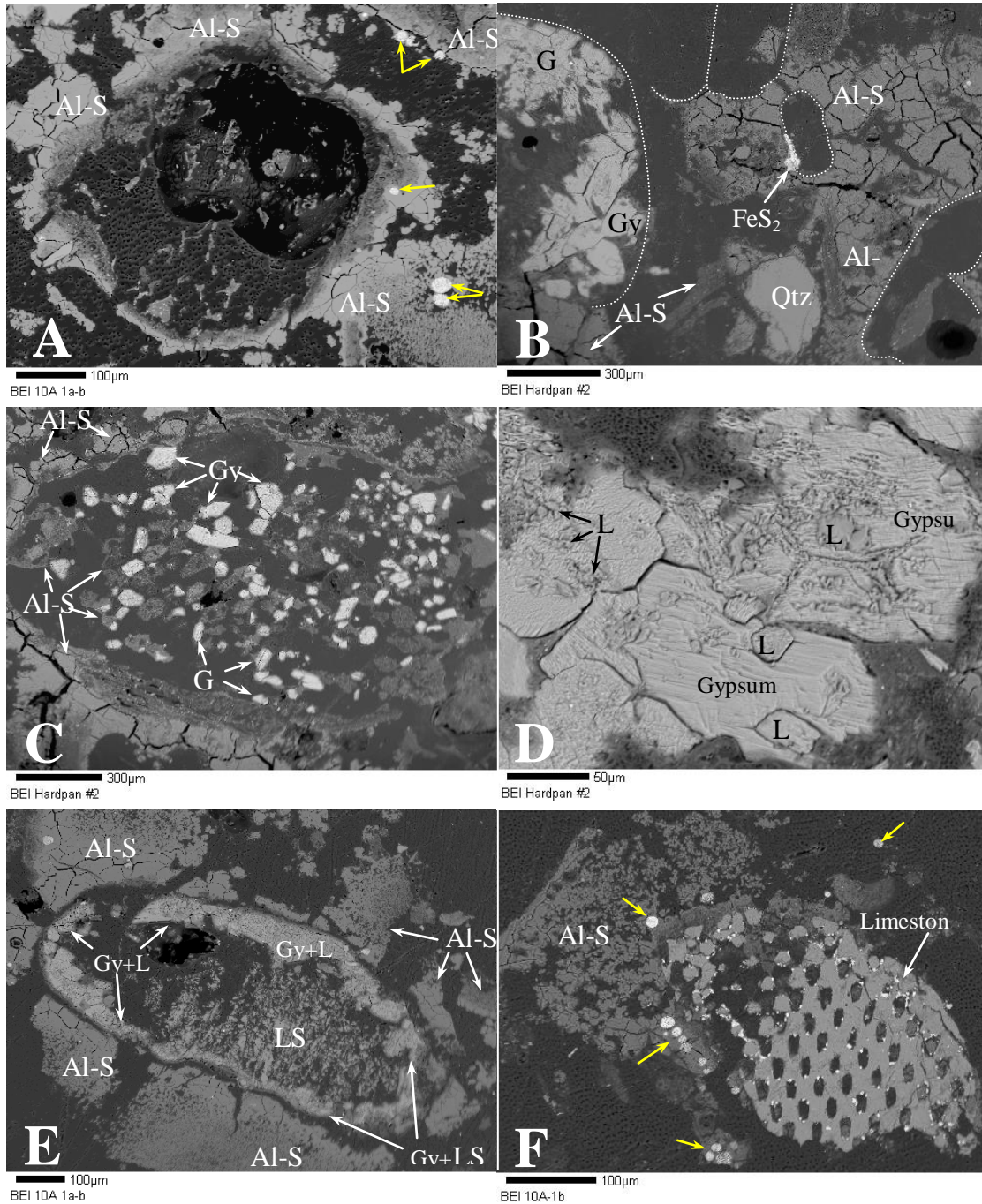
Figure 6. Photomicrographs of the transitional zone. Yellow arrows indicate framboidal pyrite. (A) Limestone ghost in the upper transitional zone rimmed by aluminum hydroxysulfate. (B) Limestone ghosts in a patch of aluminum hydroxysulfate (left) adjacent to a former limestone grain filled with blocky gypsum. (C) Aluminum hydroxysulfate and gypsum precipitated within a limestone ghost outlined by aluminum hydroxysulfate. (D) Close-up of gypsum showing intergrowth with limestone along the former limestone grain boundary. (E) Partially replaced limestone grain with a gypsum reaction rim at the former grain boundary, remnant limestone in the grain interior, and a reaction rim of aluminum hydroxysulfate separated from the former grain by approximately 5 – 10 µm. (F) Partially replaced limestone fossil rimmed by dendritic aluminum hydroxysulfate. Note the pyrite framboids framboids.

With depth, gypsum (Figure 6c) and minor amounts of remnant limestone increasingly occupy limestone ghosts. Midway through the transitional zone, remnant limestone is universal in the limestone ghosts and the abundance of aluminum hydroxysulfate and calcium sulfate precipitates peaks. Aluminum hydroxysulfate is ubiquitous; in addition to forming limestone coatings, it is precipitated within primary porosity surrounding former limestone grains and occasionally cements organic fragments together. It is notable that secondary porosity is maintained by aluminum hydroxysulfate reaction rims around limestone ghosts. Crystalline gypsum is always found within the boundaries of a former limestone grain, although organic fragments midway though the transitional zone are found permineralized by calcium sulfate (Thomas, 2002). Small (<10 μm) remnant fragments of limestone are found commonly engulfed by the gypsum (Figure 6d). The gypsum-limestone intergrowth is found along the former limestone grain boundary (Figure 6e); most interior gypsum is devoid of trapped limestone and commonly coated by aluminum hydroxysulfates.

Gypsum is generally not found in the lower half of the transitional zone and the abundance of aluminum hydroxysulfates decreases with depth. At the bottom of the transitional zone, limestone is pristine, exhibiting few signs of dissolution, aluminum hydroxysulfate coatings are sparse, and pyrite framboids suddenly ubiquitous (Figure 6f). Pyrite framboids (yellow arrows, Figure 6) are scarce in the upper portions of the transitional zone, but exhibit a trend of increasing abundance with depth, concomitant with the disappearance of iron oxyhydroxides. The pyrite framboids are small (10 – 30 μm diameter), well-crystallized, and largely associated with aluminum hydroxysulfate and limestone fragments (Figure 6f). Iron sulfides are the only metal sulfide found in the transitional zone.

Sulfide zone. The sulfide zone is characterized by a sharp decrease in the amount of aluminum hydroxysulfates, largely pristine limestone, and a plethora of iron sulfides (Figure 7). There is no gypsum. Thus, the delineating components of the sulfide zone are the absence of gypsum and the abundance of iron sulfide. In the upper portions of the sulfide zone, aluminum hydroxysulfate textures are indistinguishable from the overlying transitional zone, largely occurring as reaction rims with dendritic overgrowths around quartz, organic fragments, and
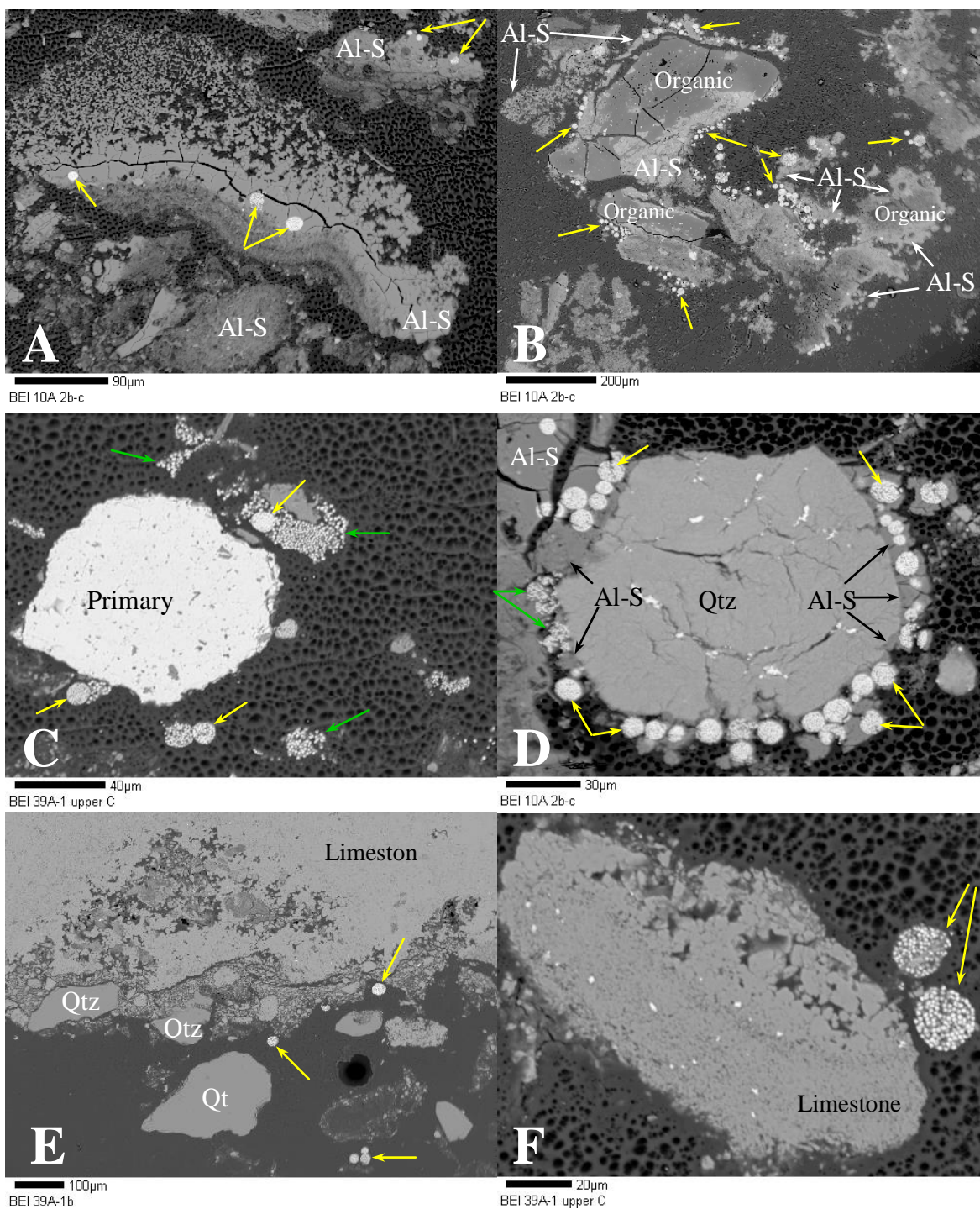
Figure 7. Photomicrographs of the sulfide zone. Yellow arrows indicate framboidal pyrite, green arrows indicate loose clusters of fine-grained (<1µm) pyrite. (A) Band of aluminum hydroxysulfate with framboid inclusions. (B) Organic matter surrounded by framboidal pyrite and permineralized by aluminum. (C) Large anhedral pyrite surrounded by individual pyrite crystallites and framboids. (D) Quartz grain coated with aluminum hydroxysulfate containing abundant framboid inclusions. (E) Lower portion of the sulfide zone showing pristine limestone. Note the similarity to figure 4c. (F) Pristine limestone grain with framboidal pyrite.

partially dissolved limestone (Figure 7a). Additionally, organic fragments are often found permineralized by aluminum hydroxysulfate (Figure 7b). As the amount of aluminum hydroxysulfate diminishes with depth, the predominant habit shifts from reaction rims associated with limestone alteration to permineralization of organic substrates.

Pyrite framboids are ubiquitous in the sulfide zone, however they are largely concentrated in clusters and proximal to grain surfaces (i.e., limestone, quartz, or wood) or former grain surfaces (yellow arrows, Figure 7c&d). As such, framboids are found intimately associated with aluminum hydroxysuylfate in the upper reaches of the sulfide zone. Notably, pyrite is commonly encapsulated by aluminum hydroxysuylfate (Figure 7a&d) indicating framboid formation precedes aluminum precipitation in paragenetic sequence. Sulfide content is greatest at the top of the sulfide layer, gradually tapering with depth. In the lower reaches of the sulfide zone framboids are found in close proximity to limestone grains (Figure 7e&f) and organic fragments, or within wood vesicles (see Thomas, 2002). Although framboids are the dominant iron sulfide habit in the sulfide zone, loose collections of very small (<1µm) pyrite spheres are also occasionally noted (green arrows, Figure 7c&d). The tiny spheres are identical in size and shape to the individual pyrite crystallites of the framboids. Large (>50µm), single, anhedral pyrite grains were rarely encountered (Figure 7c) in the sulfide zone. Large, non-framboidal iron sulfide is likely inherited from the limestone in the original substrate. Minor trace metal sulfides (e.g., cobalt, nickel, and zinc) were also identified in this zone (Thomas, 2002). Although the black color that distinguishes this zone is likely attributable to iron monosulfides (i.e., amorphous FeS, mackinawite, greigite), no iron monosulfide compounds were detected using the electron microprobe. Hand samples of the sulfide zone are highly reactive, turning from black to orange-brown within an hour upon exposure to air, and consequently were not well suited for XRD analysis. Samples selected for XRD analysis yielded only peaks attributable to limestone.

Discussion

The mineralogical zonations observed in this and other VFW studies (i.e., Watzlaf, 1997) are the result of a unique acid neutralization process, characteristic of low-pH (<3.0), ferric iron-dominated ($Fe^{+3} \gg Fe^{+2}$) ARD, which occurs within the VFW organic substrate. The dominant mechanism of metal removal is abiotic hydrolysis and precipitation due to the rapid rise in pH

(from 2.4 to 6.4).   Metal retention occurs in three zones that define the limestone dissolution front overlying a fourth zone of unreacted material.   The layering is dynamic and, as the dissolution front advances with the consumption of limestone, the layers evolve (e.g., Watzlaf, 1997; Thomas and Romanek, 2002).   Above the dissolution front (oxide zone), limestone is completely dissolved from the substrate.   Below the front (sulfide zone), limestone is pristine and largely unreacted.   The mineralogical transition zone between the oxide and sulfide layers is the area of active limestone dissolution as evident by the partially dissolved and replaced limestone (Figure 6).

Influent Chemistry and the Initial Substrate

The influent ARD chemistry and the fine-grained size (1.23 mm) of the limestone screenings are the two key contributors to the metal removal capacity of the LBOS.   The LBOS-amended VFW thrives at pH prohibitive to long-term RAPS implementation.   At the influent pH (2.4), limestone dissolution is limited only by the diffusion of hydrogen ions (Plummer et al., 1979). Moreover, the presence of ferric iron and aluminum in the influent enhances limestone dissolution via hydrogen ion generation resulting from hydrolysis and precipitation (Thomas and Romanek, 2002).   If the influent pH had been higher (>4.0), the amount and rate of limestone would have been largely controlled by the influent pCO_2 (e.g., Hedin et al., 1994b).   If the influent was dominated by ferrous iron, then much of the influent acidity would have been permitted to pass through the LBOS unfettered.

Although less than 0.5% of the limestone screenings pass through a 75 μm sieve (as reported from the quarry), electron microprobe photomicrographs of the original substrate show that very fine grained (<10 μm) limestone fragments form ubiquitous coatings on all large grain surfaces (e.g., quartz, organic fragments, and large limestone grains).   The screenings are separated from coarse limestone rock at the quarry by wet centrifugation in a cyclone vortex separator (Frank Manos, Martin Marietta, pers. comm., 2002).   Fines are then elutriated by floatation, although apparently some of the very fine grained limestone fragments adhere to the screenings.   Upon homogenization with the organic material in the cement mixer, much of the attached limestone fines are dispersed, adhering to almost every surface (e.g., quartz, organic fragments, and large limestone grains).   Attrition during mixing can be discounted as a source of the limestone fines because the duration of mixing was short (<2 minutes) and the bulk of the material in the mixer

(75% by volume) was soft, organic matter. Regardless of source, the distribution of the limestone fines greatly increases the reactive surface area in the LBOS.

Pore Water Chemistry

The discrepancy between swamper and peeper samples can be attributed to the methodology and not variation in the LBOS. The swamper allowed for spot sampling the pore water of the LBOS at predetermined intervals. The ability to discretely sample those intervals was limited, because the vacuum extraction of pore waters likely pulled water from above and below the sampling depth. This can explain the higher degree of variability in the samples taken just below the substrate-water interface compared to samples taken deeper in the LBOS (Figures 2-3). The swamper was also affected by clogging of the metal fritt. Consequently, the swamper was often removed and sonicated several times during the sampling of a particular depth. Once cleaned, the swamper was reinserted into the LBOS in an undisturbed location proximal to the previous location and the remaining sample was collected. This resulted in a very average sample taken for a given depth in a given area of the VFW. In contrast, although the peeper was installed and left undisturbed, the flat, rigid nature of the peeper likely resulted in some degree of preferential flow. This can explain the more gradual increase in pH observed in the peeper samples compared to the swamper samples (Figure 2). Spikes in dissolved iron, aluminum, and calcium observed in the peeper samples are believed to be real and not the result of preferential flow. The lack of any noticeable spike in the swampers data is attributed to the general homogenization of the swamper sample.

Development of the Dissolution Front

The swamper and peeper data demonstrate that the pore water pH increases dramatically across the limestone dissolution front (Figure 2). Metal removal coincides with the rapid change in pH. The gradual development of the limestone dissolution front begins as soon as the influent ARD makes initial contact with the LBOS. The low pH of the influent results in rapid dissolution of the fine-grained limestone (e.g., see Rose, 1999), a responsive increase in pH, and rapid hydrolysis and precipitation of iron and aluminum (e.g., see Sterner et al., 1998). The dendritic habit of both aluminum hydroxysulfate (Figures 9a & 10a) and iron oxyhydroxide

(Figure 5a-b) provides textural evidence for the rapid hydrolysis and precipitation of aluminum and iron.

Although iron and aluminum minerals coat limestone, dissolution goes to completion before the limestone is passivated through armoring, due to fine grain-size of the screenings; limestone ghosts are all that remain in the oxide zone (Figure 5). The oxide zone is the end product of limestone dissolution; it is what is left behind as the dissolution front advances deeper into the LBOS. With near complete removal of limestone, the acid neutralizing capacity of the oxide zone is reduced by greater than 90% (Thomas and Romanek, 2002). Thus, the oxide zone can be considered spent substrate that has little neutralizing or metal removal ability.

As the limestone is consumed and the dissolution front advances, the pH in the oxide zone drops and approaches influent levels (i.e., Figure 2). This ultimately leads to the development of the transitional zone and the segregation of aluminum from iron. Separation of iron and aluminum is based largely on the difference in solubility between pH 3 – 4. Ferric iron is highly soluble only below a pH of approximately 3 – 3.5 (Hedin et al., 1994a; Rose and Cravotta, 1998; Stumm and Morgan, 1981), while aluminum is highly soluble up to a pH of approximately 4 with minimum solubility not reached until pH 5 – 8 (e.g. Hedin et al., 1994a; Stumm and Morgan, 1981). Following the removal of limestone from the oxide layer, the pH remains high enough for efficient iron oxyhydroxide precipitation, but lower than that required for aluminum hydroxysulfate precipitation. Hence, precipitated aluminum compounds are continually dissolved and reprecipitated with the migration of the limestone dissolution front. Dissolution of aluminum from the oxide zone is reflected in the aluminum spike at pH ~ 3.8 observed in the peeper pore water analysis. In comparison to the aluminum reaction rims surrounding partially dissolved limestone in the transitional zone, the aluminum rims in the bottom of the oxide zone are less dense and partially dissolved. Secondary calcium minerals (e.g., gypsum) are also removed as the dissolved calcium concentration in the oxide zone decreases concomitant with the advancement of the limestone dissolution front. Thus, there is no gypsum present in the oxide zone, although gypsum ghosts indicate their former presence (Figure 5f).

The transitional layer is the zone of active limestone dissolution and is the source of all the limestone-related textures; there is no limestone present above the transitional zone and the limestone below is pristine. Thus, the transitional zone is pronounced in the peeper pore water samples by the peak in calcium concentration (Figure 3). The isolated presence of gypsum in the

transitional zone also indicates that the concentration of dissolved calcium and/or sulfate was highest in the transitional zone. Once the transitional zone is established and separated from the oxide zone, all of the evidence of limestone dissolution is preserved by aluminum and calcium hydroxysulfates. As indicated from the oxide zone these precipitates are transient, dissolving and reprecipitating with the advancing limestone dissolution front. Hence, the transitional zone is ephemeral; the advancing oxide zone obliterates evidence of its former existence.

The dynamic and transitory nature of the transitional zone is important to the longevity of the system. In hand samples, the transitional zone is demarcated by a hardpan of aluminum and calcium hydroxysulfates surrounding partially dissolved limestone. Petrographic evidence indicates that the permeability of the hardpan is maintained through secondary porosity created by the removal of limestone. Moreover, once the limestone is removed, the pH and calcium concentration decreases to the point where the minerals forming the hardpan are soluble.

Peeper data indicate iron is also solubilized in the lower oxide zone and upper parts of the transitional zone (Figure 2). The spike in iron coincides with the transition from ferric iron-dominated influent to ferrous iron-dominated pore water and a shift in the iron removal mechanism from oxyhydroxide to sulfide. The increase in ferrous iron can be assigned two potential sources. Encroachment of low pH ARD into the upper transitional zone will lead to the dissolution of the acid volatile iron monosulfides and the subsequent release of ferrous iron. While indicated in hand sample, iron monosulfides were not detected with the electron microprobe and, hence, a monosulfide source of the ferrous iron could not be evaluated texturally. Characteristically acid volatile, iron monosulfides are sensitive to decreases in pH and, hence, will likely dissolve and reprecipitate with the advancing dissolution front. Alternatively ferric iron (dissolved or as oxyhydroxide) may be reduced in the upper transitional zone via abiotic reaction with hydrogen sulfide and/or dissimilatory microbial reduction. The pH at peak iron concentrations is approximately 4.3, which is low enough to induce the dissolution of most acid volatile sulfides. However, microbial investigations of the transitional zone (Thomas, 2002) also indicate that abundant, viable iron-reducing microorganisms present the potential for dissimilatory iron reduction.

The rapid removal of dissolved iron below peak pore water concentration is attributed to bacterial sulfate reduction. Dissolved iron penetrating beyond the zone of limestone dissolution reacts with biogenic sulfide to produce abundant pyrite framboids. It is notable that pyrite is

absent from the majority of the oxide zone, found only in the lower portions; either pyrite never precipitated in the oxide layer or it has been removed. Potential loss of pyrite from the oxide layer has significant implications for the long-term retention of iron sulfide in the LBOS. Pyrite removal may be achieved through two possible mechanisms: physical transport or dissolution. Pyrite occurs as small (<1μm) spheres, predominantly clustered into framboid structures. The framboids are intimately associated with limestone or other larger fragments coated with limestone (e.g., quartz, wood fragments) and, in most instances, appear to precede the formation of any armoring aluminum precipitates. Consequently, pyrite, originally precipitated on and around limestone fragments, is commonly found engulfed and matrix-supported by aluminum hydroxysulfates (Figure 7a & d). With complete limestone removal, the framboids are left suspended in the disintegrating remains of the aluminum reaction rim. Dissolution of the aluminum matrix could result in the dissociation of the framboid into individual pyrite crystallites, that could be flushed from the oxide zone. Pyrite that is not physically removed is subject to attack by influent ferric iron:

$$FeS_2 + 14\ Fe^{3+} + 8\ H_2O \Leftrightarrow 15\ Fe^{2+} + 2\ SO_4^{2-} + 16\ H^+ \qquad (1)$$
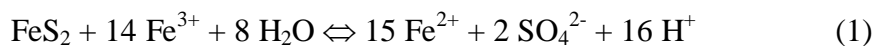
Therefore, iron sulfide removal is considered temporary and not anticipated to play a major role in long-term iron retention.

Conclusions

Complete removal of iron and aluminum from low pH (<3), ferric iron-dominated (Fe^{3+} » Fe^{2+}) ARD is possible with a limestone-buffered organic substrate (LBOS) without armoring and passivation of the limestone. Iron is removed as both oxyhydroxides and sulfides, but the fine-grained iron sulfides are likely transient while the oxyhydroxides may represent more permanent removal. The circumneutral pH below the limestone dissolution front assures that aluminum removal is complete. However, when the limestone dissolution front reaches the bottom of the LBOS, a very large pulse of aluminum is expected, after which aluminum will no longer be retained. Previous studies (Watzlaf, 1997) have shown a similar pattern of iron and aluminum removal. We propose that the formation of an oxide zone characterized by iron oxyhydroxides,

very low neutralizing potential, and minimal amounts of aluminum; a transitional zone dominated by aluminum precipitates and active consumption of the substrate neutralization potential; and a zone of active sulfate reduction (sulfide zone) are attributes common to VFW treating low pH (<3), ferric iron-dominated ($Fe^{3+} \gg Fe^{2+}$) ARD.

Acknowledgements

Literature Cited

Anderson, M.A., 1990. A Hydrogeochemical Investigation of Metalliferous Coal Pile Runoff and Its Interaction with Soil and Groundwater. Ph.D. Thesis, Virginia Polytechnic Institute and State University, Blacksburg, VA, 124 pp.

Anderson, M.A., Bertsch, P.M., Feldman, S.B. and Zelazny, L.W., 1991. Interactions of acidic metal-rich coal pile runoff with a subsoil. Environ. Sci. Technol., 25(12): 2038-2046. http://dx.doi.org/10.1021/es00024a008.

American Public Health Association, 1998. Standard Methods for the Examination of Water and Wastewater. APHA, Washington, D.C., 1268 pp.

Eger, P., 1992. The use of sulfate reduction to remove metals from acid mine drainage, Proceedings of the 9th Annual National Meeting of the American Society of Surface Mining and Reclamation, Duluth, Minnesota, pp. 563-578.

Hedin, R.S., Narin, R.W. and Kleinmann, R.L.P., 1994a. Passive treatment of coal mine drainage. Bur. of Mines, Inf. Circular IC9389, US Dept. of Interior, Bureau of Mines, Washington, DC.

Hedin, R.S., Watzlaf, G.R. and Narin, R.W., 1994b. Passive treatment of acid mine drainage with limestone. J. Environ. Qual., 23: 1338-1345. http://dx.doi.org/10.2134/jeq1994.00472425002300060030x.

Hesslein, R.H., 1976. An in situ sampler for close interval pore water studies. Limnol. Oceanogr., 21: 912-914. http://dx.doi.org/10.4319/lo.1976.21.6.0912.

Millings, V.E., 1999. Stable isotopes as groundwater tracers at the D-Area Coal Pile Runoff Basin of the Savannah River Site, Aiken, SC. MS Thesis, University of Georgia, Athens, GA, 131 pp.

Plummer, L.N., Wigley, T.M.L. and Parkhurst, D.L., 1979. Critical review of the kinetics of calcite dissolution and precipitation. In: E.A. Jenne (Editor), Chemical Modeling in Aqueous Systems - Speciation, Sorption, Solubility, and Kinetics. Am. Chem. Soc. Symp. Ser. 93, Washington, DC, pp. 537-573. http://dx.doi.org/10.1021/bk-1979-0093.ch025.

Rose, A.W. and Cravotta III, C.A., 1998. Geochemistry of Coal Mine Drainage. In: K.B.C. Brady, M.W. Smith and J. Schueck (Editors), Coal Mine Drainage Prediction and Pollution Prevention in Pennsylvania. The Pennsylvania Department of Environmental Protection, Harrisburg, pp. 1-1 to 1-22.

Sterner, P., Skousen, J. and Donovan, J., 1998. Geochemistry of laboratory anoxic limestone drains. In: D. Throgmorton, J. Nawrot, J. Mead, J. Galetovic and W. Joseph (Editors), Proceedings of the 15th Annual National Meeting of the American Society of Surface Mining and Reclamation, St. Louis, MO, pp. 214-234.

Stumm, W. and Morgan, J.J., 1981. Aquatic Chemistry. John Wiley & Sons, New York, 780 pp.

Thomas, R.C., 2002. Constructed treatment wetlands in the remediation of acid rock drainage: Mechanisms of metal removal and acid neutralization, microbial ecology, and design innovations. Ph.D. Thesis, University of Georgia, Athens, GA, in prep pp.

Thomas, R.C. and Romanek, C.S., 2002. Passive treatment of low-pH, ferric iron-dominated acid rock drainage in a vertical flow wetland I: Acidity neutralization and alkalinity generation,

Proceedings of the 19th Annual National Meeting of the American Society of Surface Mining and Reclamation. ASMR, Lexington, KY, pp. these proceedings.

To, T.B., Nordstrom, D.K., Cunningham, K.M., Ball, J.W. and McCleskey, R.B., 1999. New method for the direct determination of dissolved Fe(III) concentration in acid mine waters. Environ. Sci. Technol., 33(5): 807-813. http://dx.doi.org/10.1021/es980684z

Watzlaf, G.R., 1997. Passive treatment of acid mine drainage in down-flow limestone systems. In: J.E. Brandt (Editor), Proceedings of the 14th Annual National Meeting of the American Society of Surface Mining and Reclamation., Austin, TX, pp. 611-622.

Winger, P.V. and Lasier, P.J., 1991. A vacuum-operated pore-water extractor for estuarine and freshwater sediments. Arch. Environ. Contam. Toxicol., 21: 321-324. http://dx.doi.org/10.1007/BF01055353.